PROCEEDINGS OF SCIENCE

Polarization transmission to high energy at the EIC's HSR

Eiad Hamwi,[a,*] **Georg H. Hoffstaetter,**[a,b] **Kiel Hock**[b] **and Haixin Huang**[b]

[a] *Cornell University,*
Ithaca, NY 14853
[b] *Brookhaven National Laboratory,*
Upton, NY 11973

E-mail: eh652@cornell.edu

The EIC's Hadron Storage Ring will capture and accelerate spin-polarized hadron bunches from the injector chain comprising OPPIS/EBIS, Linac, Booster, and the AGS. If unaccounted for, polarized species will cross a vast number of depolarizing first-order spin-orbit resonances, which for ultra-relativistic particles occur every 523 MeV for protons, every 13.1 GeV for deuterons, every 336 MeV for helions, etc. Pairs of Siberian snakes, consisting of helical dipole magnets, are used to fix the closed-orbit spin tune at 1/2, thereby avoiding first-order spin-orbit resonances. Nevertheless, prominent higher-order spin resonances do arise in the vicinity of the strongest first-order resonances, and necessitate the use of multiple pairs of snakes for mitigation. Due to their larger anomalous g-factor, polarized helions will undergo more frequent and stronger spin resonances than polarized protons in the HSR, in a regime not yet tested by RHIC since they are not yet available. We investigate two different snake-matching scenarios for the HSR by varying the betatron phase advance between the snakes to find an accelerator lattice configuration with the highest polarization transmission.

20^{th} *International Workshop on Polarized Sources, Targets, and Polarimetry*
22-27 September, 2024
Jefferson Lab, Newport News, VA, USA

*Speaker

PoS(PSTP2024)023

1. Introduction

The acceleration of polarized beams in particle accelerators and colliders faces many challenges, especially to very high energies. These challenges lie in both the production of polarized beams as well as their transport and acceleration, where this paper addresses obstacles in the latter for the case of hadrons. The Hadron Storage Ring at the upcoming Electron Ion Collider will accelerate polarized protons to 275 GeV and polarized helions (helium-3 nuclei) to around 180 GeV/nucleon. The only comparable energies to which polarized beams have been accelerated to are 255 GeV for polarized protons at the Relativistic Heavy Ion Collider. Helium-3 is quite a new species for polarized acceleration, and faces more difficulties due to its much larger anomalous magnetic moment of $G \sim -4.184$, compared to protons' $G \sim 1.793$. In an overly simplified way, there are approximately $4.184/1.793 \approx 7/3$ more challenges per unit relativistic γ (in the form of first-order spin-orbit resonances) to reach polarization at high energy, but due to helium-3's higher rigidity (at fixed γ) this ratio is somewhat decreased. Overall, at maximum energy, helium-3 beams will have crossed around 800 imperfection and 1600 intrinsic resonances, compared to proton beams' 525 imperfection and 1050 intrinsic resonances. Combined with the increase in strength of these resonances at higher $G\gamma$ factors, this makes polarized helium-3 a much more challenging candidate for high-energy acceleration. The primary strategy for such acceleration is the use of Siberian snakes, which negate the conditions for these resonances, but simultaneously allow the presence of new, higher-order resonances. The secondary strategy is the minimization of emittance, which is also very helpful and is hoped to be achieved via electron cooling which should decrease normalized emittance by up to a factor of 10 in the transverse phase space [1]. This situation effectively eliminates any challenges for both polarized proton in the 2-IP lattice and polarized helion beams in the 1-IP lattice, including higher-order spin resonances [2]. Nevertheless, it is unknown whether this pre-cooler will be completed during initial construction or later as an upgrade to the base design. Without the pre-cooler, it has been shown that it is possible to accelerate polarized protons to top energy without any polarization loss, in the absence of machine errors, through the use of six Siberian snakes [3]. However, due to the larger anomalous magnetic moment of helion, in this paper we investigate other strategies for the mitigation of polarization loss for helion beams during the accelerator ramp. In particular, we explore two scenarios for minimizing depolarization.

2. Spin Transport

Due to the conserved nature of spin angular momentum of a particle, the motion of 3D semiclassical spin can always be described as precession with some torque-induced angular velocity pseudovector,

$$\frac{\mathrm{d}\vec{S}}{\mathrm{d}t} = \vec{\Omega} \times \vec{S}, \tag{1}$$

Under the influence of a magnetic field, the 3D semiclassical spin angular momentum of a motionless particle with gyromagnetic ratio $\frac{q}{2m}g$ precesses in a simple way, known as Larmor precession,

$$\vec{\Omega}_L = -\frac{q}{2m} g \vec{B}. \tag{2}$$

However, a moving spinor on a curvilinear coordinate system in the presence of electromagnetic fields will accumulate new effects due to Thomas precession. Combining these effects in a relativistic covariant way leads to the well-known Thomas-Bargmann-Michel-Telegdi equation [4], which can be written as:

$$\vec{\Omega}_{\mathrm{BMT}} = -\frac{q}{\gamma m}\left[(G\gamma+1)\vec{B} - \frac{G\vec{p}\cdot\vec{B}}{(\gamma+1)m^2c^2}\vec{p} - \frac{1}{mc^2}\left(G+\frac{1}{\gamma+1}\right)\vec{p}\times\vec{E}\right], \tag{3}$$

where γ is the relativistic factor, and $G = (g-2)/2$, where g is the dimensionless g-factor of the anomalous magnetic moment. So we see that in the absence of electric fields, this equation can be rewritten in terms of transverse and longitudinal componets of $\vec{B}$ fields, $\vec{B}_\perp$ and $\vec{B}_\parallel$. Furthermore, in the context of ultra-relativistic circular accelerators without horizontal fields along the design orbit, we are left with one dominating term, which we call $\vec{\Omega}_0$ to represent the spin angular velocity on the closed orbit:

$$\vec{\Omega}_0 = -\frac{q}{m\gamma}\,(G\gamma+1)\,\vec{B}_\perp. \tag{4}$$

Finally, we see that in a stationary reference frame rotating in sync with the momentum $\vec{p}$ of the closed orbit, the angular speed (or precession rate) of the closed-orbit spin, commonly known as the *closed-orbit spin tune* ν_0 is

$$\nu_0 \equiv \left|\vec{\Omega}_0\right| = \frac{|qG|}{m}\left|\vec{B}_\perp\right| = G\gamma\ [\mathrm{rev/turn}]. \tag{5}$$

3. Spin-Orbit Resonance

3.1 First-order resonances

Conditions arise that can trigger resonant effects in a bunch's spin precession. Particularly, natural deviations in magnet alignments and magnetic field strengths give rise to *imperfection resonances* if the expected closed-orbit spin tune ν_0 is an integer, i.e. if the polarization vector is unchanged turn-by-turn:

$$\nu_0 = G\gamma \in \mathbb{Z}. \tag{6}$$

This subjects the bunch polarization to the same perturbations every turn, leading to exponential decoherence of polarization.

Otherwise, natural vertical betatron oscillations subject the particles in a bunch to horizontal transverse fields in a quasi-periodic manner, possibly leading to depolarization. These effects are known as *intrinsic resonances* since they arise from the strong focusing of alternating gradient accelerators, and occur if the closed-orbit spin tune ν_0 synchronizes with the vertical betatron tune Q_y:

$$\nu_0 \pm Q_y \in \mathbb{Z}. \tag{7}$$

3.2 Avoiding resonances with Siberian snakes

Siberian snakes are special-function magnets that were conceived in Novosibirsk in the late 1970s by Ya. S. Derbenev and A. M. Kondratenko [5, 6]. They are used to rotate the spin of

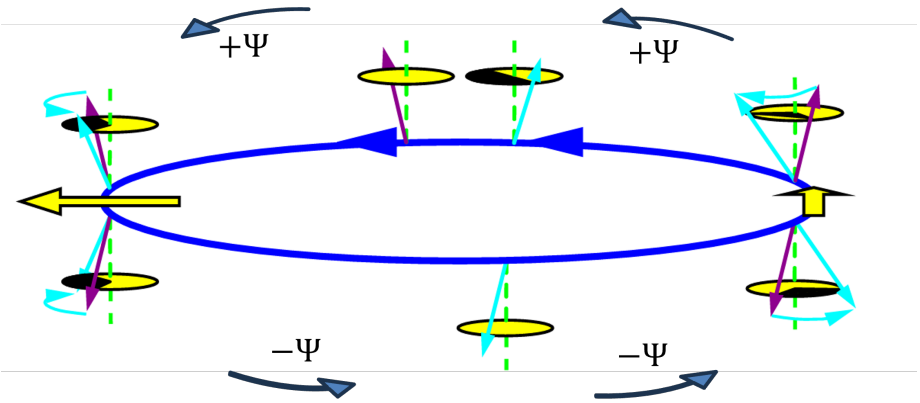

Figure 1: Schematic snake mechanism representation, where the accelerator closed-orbit is represented by the central blue circle, fibered by the magenta (early) and cyan (late) spin vectors as well as yellow circles indicating the spin phase advance as black shading. The snakes themselves are the yellow arrows on the closed-orbit, oriented parallel to their axes of rotation. The image shows a perspective projection from ~ 30° above horizontal.

particles with large $G\gamma$-factors by 180° during acceleration. The name "Siberian snake" was coined by E. D. Courant and refers to the helical shape of the beam path in the device.

By rotating the spin around a horizontal axis, pairs of diametrically opposite snakes can be used to fix $\nu_0 = \frac{1}{2}$.

The necessary conditions for this phenomenon are that the integrated vertical spin precession through dipoles $\Delta\Psi$ is zero, and the total vertical spin precession through snakes is exactly 180°. Together, these conditions allow $\nu_0 = \frac{1}{2}$ to be true independently of energy. A schematic representation, adapted from [7], is shown in Fig. 1.

3.3 Invariant Spin Field

The proper use of Siberian snakes enables the beam to avoid all first-order spin resonances, both imperfection and intrinsic, due to fixing the closed-orbit spin tune ν_0.

However, in stable beam dynamics there usually exists a generalized reference frame describing the spin precession of particles away from the closed-orbit, known as the *invariant frame field* [8]. In particular, the axis $\vec{n}(\vec{z}, s)$ corresponding to vertical on the closed-orbit, referred to as the *invariant spin field* (ISF), satisfies a spin-orbital relation,

$$\vec{n}(M(\vec{z}), s) = R(\vec{z}, s)\vec{n}(\vec{z}, s), \tag{8}$$

where s is the azimuthal position, $\vec{z}$ is the 6D phase space position, $M(\vec{z}, s)$ is the 1-turn orbital map, and $R(\vec{z}, s)$ is the 1-turn spin rotation matrix.

In this coordinate system, the generalized precession frequency around n is termed the *amplitude-dependent spin tune* ν and is in general different from the closed-orbit spin tune,

$$\nu \neq \nu_0 = \frac{1}{2}. \tag{9}$$

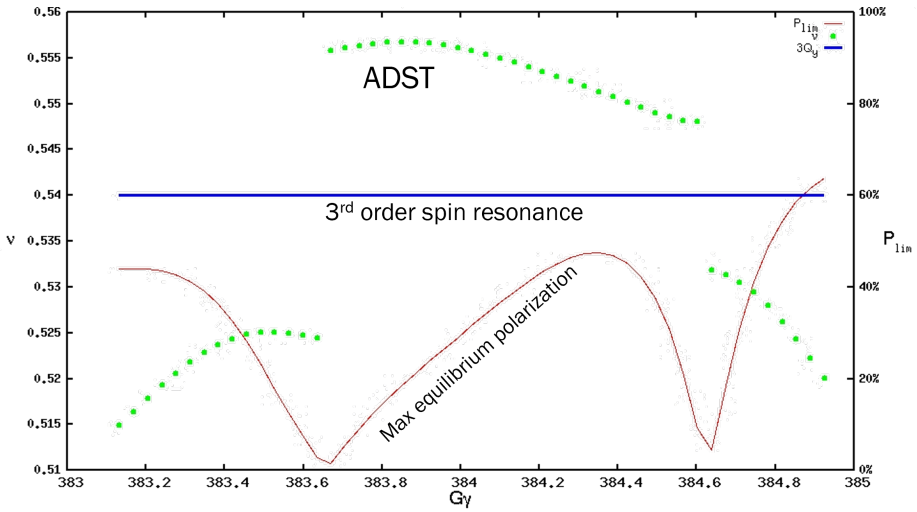

Figure 2: Example 3rd-order spin resonance on a high-amplitude torus from the RHIC lattice ($[Q_y] = 0.18$).

3.4 Higher-order resonances

In this coordinate system, we find new, higher-order spin-orbit resonances arising from non-linearities in the spin-orbit coupling integrals. Among these higher-order resonances are the well-known *snake resonances*, occurring for specific choices of vertical orbital tune that generate fundamental discontinuities in the invariant spin field. Overall,

$$\nu + j_x Q_x + j_y Q_y + j_z Q_z = k, \qquad \vec{j}, k \in \mathbb{Z}, \tag{10}$$

is a set of conditions for such higher-order resonances to occur. A specific example of such a higher-order resonances is shown in Fig. 2.

By choosing appropriately irrational tunes, higher-order resonances can be avoided for small amplitude particles. Higher-order spin resonances are found in the energy vicinity of major first-order spin resonances due to their strong spin-orbital perturbations. The only way to confirm the presence of higher-order resonances is via computationally expensive, non-perturbative methods (Stroboscopic averaging, SODOM-2, etc.) [9, 10].

3.5 Spin-orbit coupling

To gain a handle on higher-order resonant spin motion, it is instructive to consider significant first-order motion. Experience has demonstrated that in vicinities of energy nearing strong first-order spin resonances, higher-order spin resonances are commonly found in the presence of snakes that eliminate the first-order resonance, especially at large orbital amplitudes. In a linearized approximation of spin-orbit motion, the cumulative effect of non-vertical spin precession is referred to as *spin-orbit coupling*. Such coupling arises due to motion in quadrupoles, sextupoles, etc., as well as coupled optics, but typically only considers quadrupole effects as these are dominant in most cases. To calculate the contributions, one needs to integrate the spin precession vector away from the closed-orbit, $\vec{\omega} = \vec{\Omega} - \vec{\Omega}_0$, but also modulated by the spin phase advance $\Psi(s) = \int_0^s \vec{\Omega}_0(s) \cdot \vec{n}_0(s)\, \mathrm{d}s$,

$$\Delta(s_x + i s_y) \propto \oint_{l_0}^{l_0+L} [\vec{\omega}(s) \cdot (\hat{x} + i\hat{z})]\, e^{-i\Psi(s)}\, \mathrm{d}s, \tag{11}$$

which can be further approximated in linearized orbital motion by,

$$\Delta(s_x + is_y) \propto (G\gamma + 1) \oint_{l_0}^{l_0+L} k(s)\sqrt{\beta_y(s)}\, e^{\pm i\,\phi_y(s)} e^{-i\Psi(s)}\, \mathrm{d}s, \tag{12}$$

where $k = \frac{1}{B\rho}\frac{\mathrm{d}B_y}{\mathrm{d}x}$ is the focusing strength, β_y and ϕ_y are the betatron amplitude and phase advance, and L is the circumference of the accelerator.

4. Snake Matching

Currently, through the use of 6 diametrically opposite snakes, simulations indicate it is possible to accelerate protons to high energy without any polarization loss [3]. Other simulations indicate it will be challenging to attain such polarization at the top energy for helion beams [2]. Here we attempt to address this through the method of *snake matching*[11, 12].

Due to the computational burden of directly computing higher-order resonance strengths in the presence of snakes, a useful but indirect first step at mitigating such resonances is by minimizing the spin-orbit coupling integrals, which are equivalent to first-order resonance strengths in the absence of snakes. It is true that the snakes themselves entirely eliminate all first-order resonances by forcing the closed-orbit spin tune away from the betatron tunes, but what remains after this constraint is some non-zero coupling which is indicative of depolarizing tendencies beyond first-order.

Since the coupling is a function of energy, it will be necessary to minimize this coupling at various resonant energies, which are usually in the same energy range as the strongest first-order resonances. By considering Eq. 12, it becomes apparent that there are two clear options available to us: either vary $\Psi(s)$, or vary $\phi_y(s)$. Varying $\Psi(s)$ is possible by adjusting the rotation axis of a snake [11], and varying $\phi_y(s)$ is possible by manipulating the quadrupole strengths in the lattice.

In this paper, we focus on the latter of the two alternatives, since we claim that it is more simple to adjust betatron phase advances than to adjust snake rotation axes in general. In particular, certain rotation axes are inaccessible in the current implementation of snakes that is being used at BNL since they may demand too high of a current in the superconductors, leading to possible quenches. Furthermore, we implement two different scenarios to consider the possibility of varying the phase advances in different arcs of the ring.

4.1 First scenario

In the first scenario, we consider a realistic implementation of additional power supplies in two out of the six arcs of the HSR. Here, we use the storage lattice optics with 2 IPs [13], as opposed to the injection optics. This means the beta function has been squeezed down to $(\beta_x, \beta_y) = (80\,\mathrm{cm}, 7.2\,\mathrm{cm})$ at both the 6-o'clock and 8-o'clock interaction points (known as the 2-IP store lattice). In particular, by varying the current in just the arc quadrupoles, we can manipulate the periodic beta function in such a way as to precisely control the phase advance in the arc. All that is necessary is to appropriately match the beta and dispersion functions from the central point to the new periodic values at the beginning of the arc.

Since there are 6 arcs, we could vary the vertical phase advance in a 6-dimensional space to search for the best possible results, but this produces a vast search space and a very slow computing

task, that of evaluating the nonlinear polarization afterward. Instead, we opt to just vary the vertical phase advance in 2 of the 6 arcs, with two additional power supplies. We then use the main and trim power supply for all quadrupoles to ensure the overall tunes are held constant after changing the phase advance individually in the two arcs of choice.

Based on our own experience and the results of [2, 14], we choose the 2 arcs surrounding the active IRs. We connect the first power supply (PS-1, current I_1) to the arc quadrupoles YI6_QD10 $\longrightarrow$ YI7_QD10 between IR6 and IR8, and the second power supply (PS-2, current I_2) to the arc quadrupoles YO8_QF10 $\longrightarrow$ YI9_QF10 between IR8 and IR10. A schematic is shown in Fig. 3.

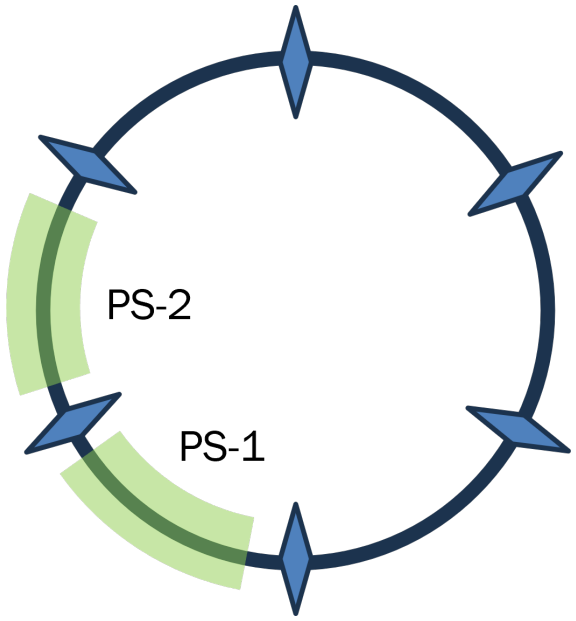

Figure 3: Schematic of 2 arc power supply shunts overlayed on the hadron storage ring lattice.

In Fig. 4 we show the amount of current necessary in each shunt power supply to achieve a certain choice of vertical phase advances in the two arcs.

Then, to evaluate the level of polarization loss at a level beyond first-order in orbital dependence, we track a single helium-3 nucleus across the most depolarizing energy range from $G\gamma = 700 \rightarrow 800$. In this scenario, we only consider ampltiudes relevant to a cooled, flat beam, but with twice the vertical amplitude: $(J_x, J_y) = (2.5\,\pi\,\text{mm mrad}, 0.5\,\pi\,\text{mm mrad})$. We initialize the spin of said particle according to the local invariant spin field direction at it's starting position, and we project the final spin vector along the final local invariant spin field. We track a single particle for each choice of phase advance in the red square in Fig. 4, and the results are shown below in Fig. 5. The ramping rate is set to $\dot{\gamma} = 0.75/\text{sec}$.

In Fig. 5, we see that slightly to the right of the working point there is a yellow island of high polarization transmission. In particular, it seems that for $\phi_{y,6-7} \geq 16.8$ the polarization transmission is almost perfect for most choices of $\phi_{y,8-9}$. This situation indicates that the working point is already close to an optimal point for cooled polarization transmission in the 2-IP lattice, which agrees with the cooled bunch tracking results for the 1-IP lattice in [2]. We show a specific example of one of these points in Fig. 6.

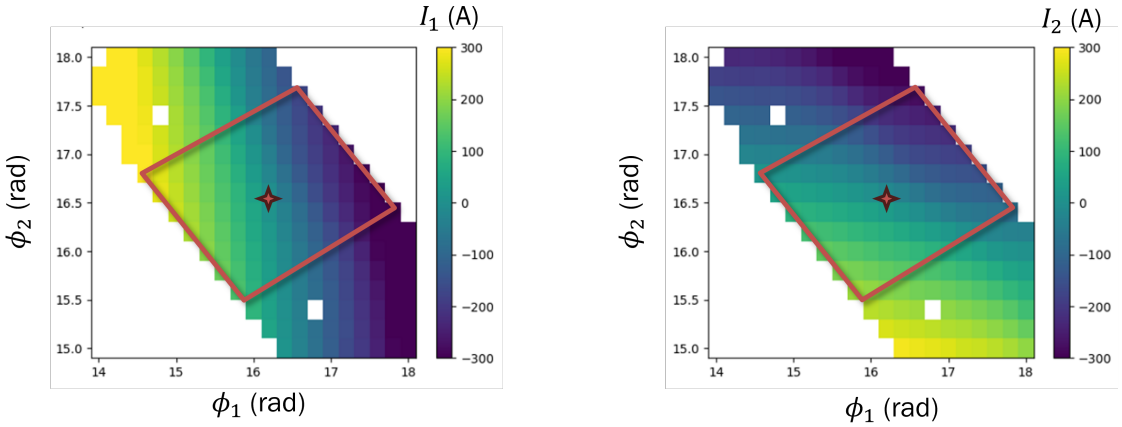

Figure 4: Power supply loads as a function of vertical phase advance. The red star in the center of each plot is the current working point. The red square highlights the regions which are evaluated for polarization transfer.

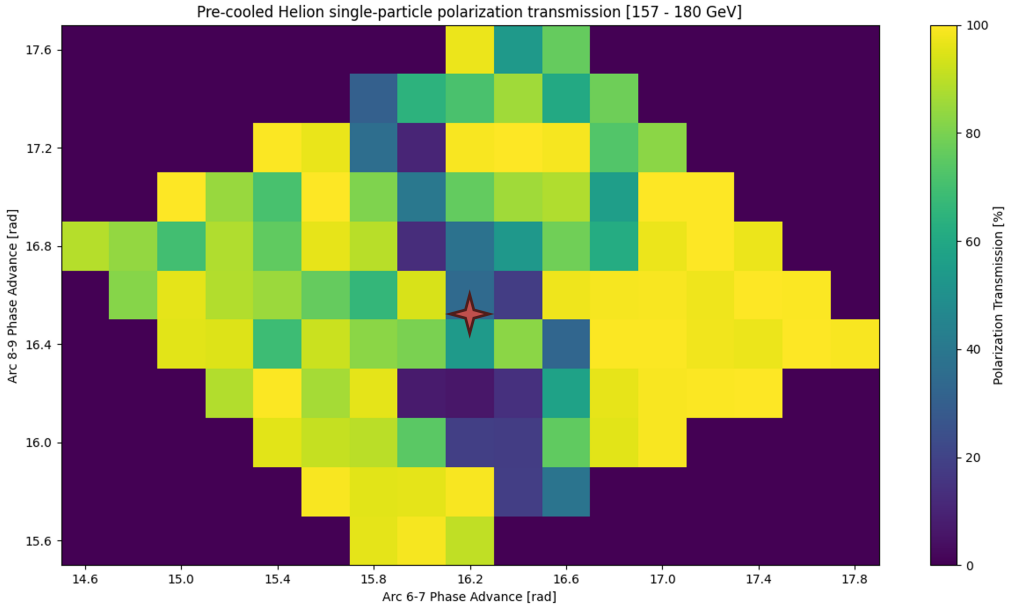

Figure 5: Cooled helion particle polarization transmission with respect to the local invariant spin field in the 2-IP lattice. The red star indicates the current working point.

4.2 Second scenario

In the second scenario, we consider a different lattice optic, specifically the injection lattice [15, 16]. The injection lattice only considers the 1-IP situation, and also has larger beta-star values of $(\beta_x, \beta_y) = (5\,\text{m}, 45\,\text{cm})$ at IP6. Furthermore, instead of actually using power supply shunts and varying the periodic beta function, we use 4×4 transverse phase space matrices distributed around the arc quadrupoles to artificially vary the phase advance in each arc, referring to them as *phase trombones*.

Then, instead of using a brute-force approach of explicitly evaluating each possible combination

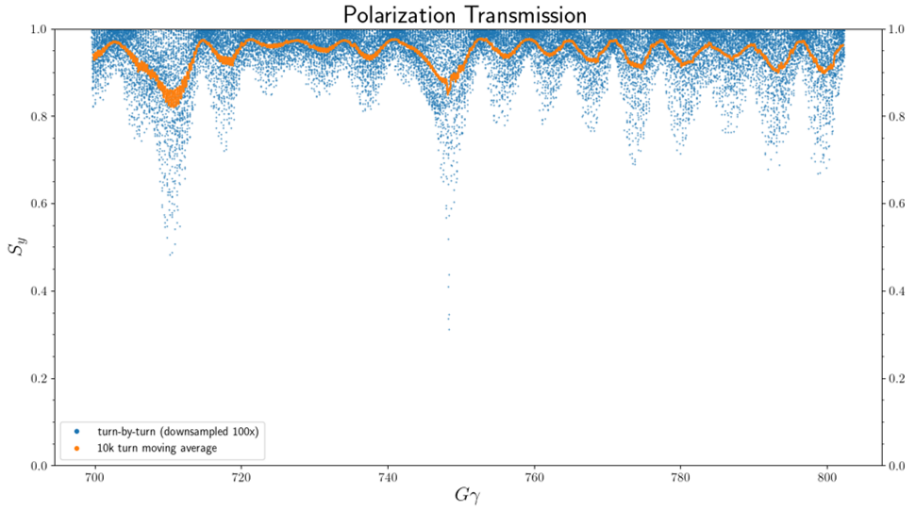

Figure 6: One example of a successful polarized ramp with 98% transmission is (16.6 rad, 16.6 rad).

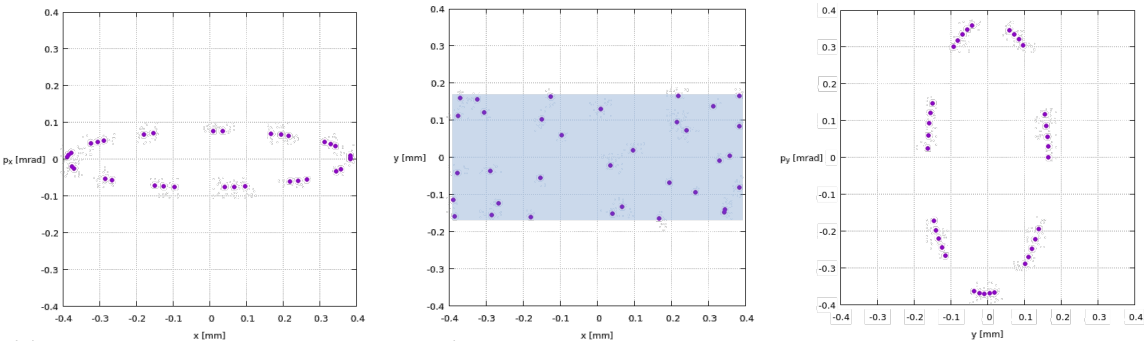

Figure 7: Phase space distribution of uncooled helium-3 bunch with $(\epsilon_x, \epsilon_y) = (2.5\,\pi\,\text{mm mrad}, 5.0\,\pi\,\text{mm mrad})$. Left plot shows horizontal phase space, center shows bunch profile, and right plot shows vertical phase space.

of phase advances that conserves the tune, we opt to use an optimization procedure based on minimizing the spin-orbit coupling integrals (introduced in Section 3.5) at various resonant energies which contribute the strongest depolarization.

Finally, we also evaluate the polarization transmission of an entire 4D bunch of particles, as opposed to a single particle in 4D space, to more accurately sample the phase space trajectories, and use the same ramping rate of $\dot{\gamma} = 0.75/\text{sec}$. We quickly find that there is no polarization loss at all for cooled helions in the injection lattice (similar to the 1-IP store lattice situation). However, significant problems show up when we consider an uncooled beam of helions at 2σ vertical emittance, with phase space distribution shown in Fig. 7.

Specifically, when considering the same energy range as before of $G\gamma = 700 \longrightarrow 800$, we find immediate depolarization due to higher-order resonance crossing at $G\gamma \sim 705$. This is mildly alleviated with the phase trombones optimized to enhance spin-orbit coupling at the $G\gamma = 705$ region, as shown in Fig. 8, but remains significantly problematic. Specifically, the polarization obtained by projecting the spins of the bunch on their local invariant spin field $\langle \vec{S} \cdot \vec{n} \rangle$ improves

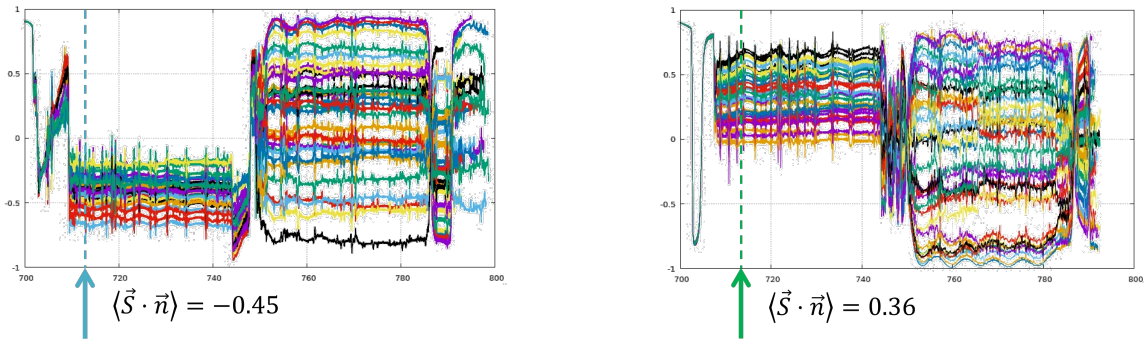

Figure 8: Averaged vertical component of spin ($\langle S_y \rangle$) for each particle in bunch. Left plot shows base lattice, right plot shows lattice with a set of correction phase trombones.

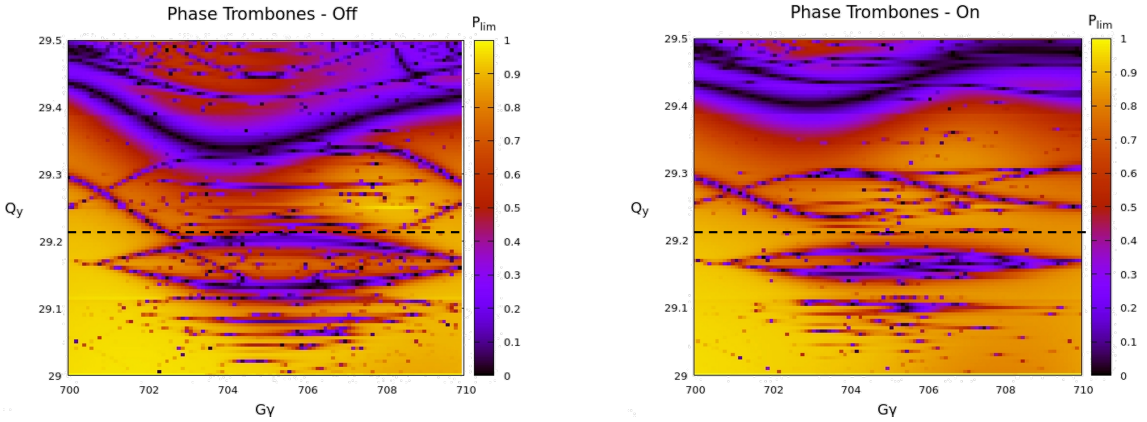

Figure 9: Plot of maximum time-averaged polarization $P_{lim}\left(J_x = 2.5\,\pi\,\mu m, J_y = 5\,\pi\,\mu m\right)$ over a tune-energy region of strong depolarization. The dashed line shows the working point of $Q_y = 29.210$. Left plot shows base lattice, right plot shows lattice with a set of correction phase trombones.

from -0.45 to 0.36.

We then consider the effect of changing the overall vertical tune of the lattice as well, in an attempt to find safer tunes during the ramp. We do this for both the base injection lattice as well as for the phase trombone enhanced lattice for comparison. The results in Fig. 9 show the maximum time-averaged polarization, which is the average of the ISF over a phase space torus of fixed amplitude $P_{lim} \equiv \langle \vec{n}(\vec{z}) \rangle$, for both lattices over the first strongly resonant region. The dark regions reflect the presence of a higher-order resonance.

We see that in both situations, the nominal tunes cross a resonant region, although the base lattice is much more strongly resonant there. In particular, the bands of higher-order resonance due to the equivalence of ν and $1 - \nu$ get tighter with the phase trombones, indicating the spread in the ADST gets smaller $\nu \to \frac{1}{2}$. Finally, we observe a narrow region of without resonance in the tune space on the right plot near $Q_y = 29.125$, which we explore further. We track the same bunch of particles using the new working point with phase trombones and find drastic improvement in the polarization transmission up to this point, shown in Fig. 10.

The situation is already improved dramatically, and we press along further. We repeat the same tune scan procedure and observe that without the phase trombones, the new tune is actually safe

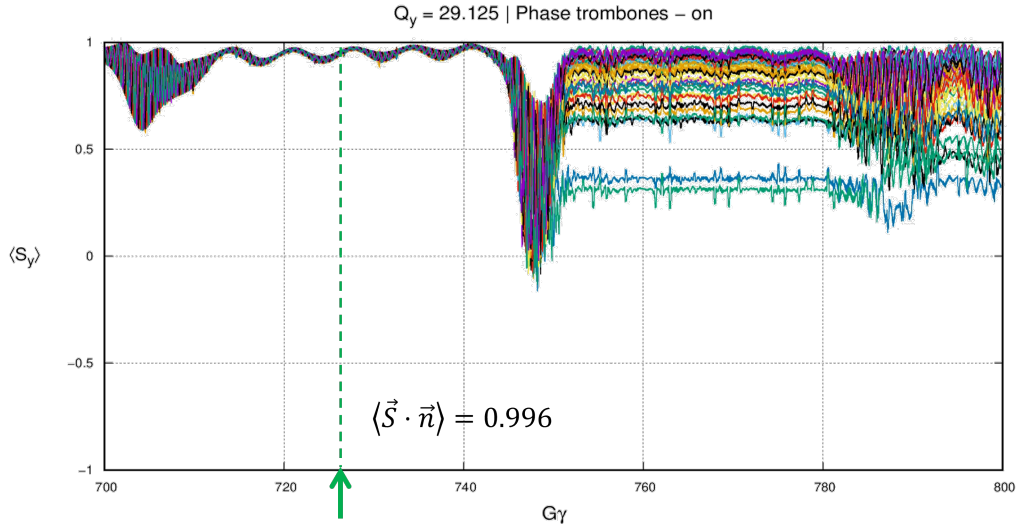

Figure 10: Averaged vertical component of spin ($\langle S_y \rangle$) for each particle in bunch, with new working point $Q_y = 29.125$ and phase trombones on.

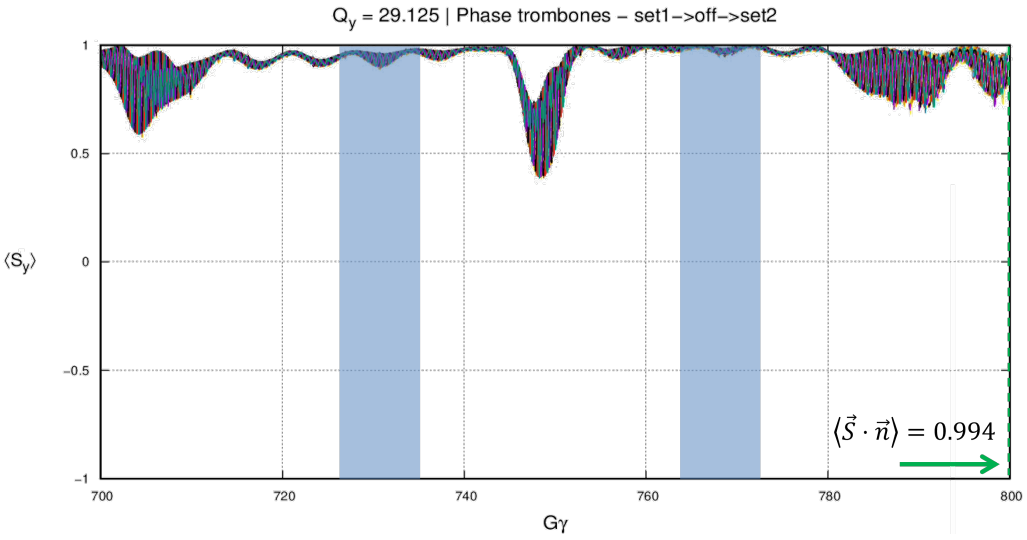

Figure 11: Averaged vertical component of spin ($\langle S_y \rangle$) for each particle in bunch, with new working point $Q_y = 29.125$ and 3 different settings for the phase trombones. The shaded blue regions indicate the time when lattice linearly interpolated between the settings.

for polarization transmission across the next strongly depolarizing region $G\gamma \sim 745$. Finally, again with the same procedure we find a new setting for the phases trombones for the tail end of our energy range $G\gamma \sim 790$. Thus, we alternate between all three settings and are able to successfully transfer 99.4% of the polarization of the bunch from $G\gamma = 700$ to $G\gamma = 800$, as shown in Fig. 11.

Here we note that the new working point of $Q_y = 29.125$ lies technically on an 8^{th} order vertical orbit resonance although it is more likely to be impacted by being close to the integer orbital resonance at 29. Furthermore, this condition also technically satisfies a 4^{th} order snake resonance condition. From this we conclude that it is ideal to avoid lingering on this working point for long to

avoid the possibility of hurting the beam quality by blowing it up or depolarizing it at other energies.

5. Conclusion

In this paper we investigated the polarization transmission of polarized helions across the most dangerous energy range of the EIC's Hadron Storage Ring accelerator lattice. We considered two different implementations of the lattice, the 2-IP storage lattice and the injection lattice, and found that with minor adjustments to the vertical phase advance in two of the six arcs it is possible to achieve high polarization transmission for cooled helion beams in the 2-IP store lattice, similar to previous results on the 1-IP store lattice.

The situation deteriorates for uncooled beams in the store lattice, so we consider the simpler and more symmetric injection lattice for the case of uncooled helion beams. In this case we consider the possibility of varying the vertical phase advance of all six arcs, but we do this in a less realistic way, that of using artificial phase trombones that do not impact the beta functions. Nevertheless we find that through the use of these phase trombones it is also possible to improve the polarization situation, albeit with the additional need of changing the working point Q_y. We note that there are challenges associated with the new working point so it is helpful to avoid using it as an operating point outside this energy range. Finally, in this paper we do not consider at all the possibility of changing the snake rotation axes as additional variables for optimization, since these would drastically enlarge our optimization search space. Nevertheless, including such snake variables in a future optimization is sure to enhance the overall situation for polarization transmission.

6. Acknowledgements

I would like to thank Vadim Ptitsyn, Vahid Ranjbar, and Vincent Schoefer for helpful discussions about polarization transmission, and further thanks to J. Scott Berg and Henry Lovelace III for helpful discussions about lattice implementation and providing the accelerator lattices. Finally, I would like to thank David Sagan for his tireless efforts in building and supporting the Bmad simulation library[17], without which this work would not have been possible.

This work has been supported by Brookhaven Science Associates, LLC under Contract No. DE-SC0012704 with the U.S. Department of Energy, and No. DE-SC0018008.

References

[1] A.V. Fedotov, D. Kayran and S. Seletskiy, *Accelerator Physics Requirements for Electron Cooler at the EIC Injection Energy*, in *Proc. COOL2023*, no. 14 in International Workshop on Beam Cooling and Related Topics, pp. 1–4, JACoW Publishing, Geneva, Switzerland, 4, 2024, DOI.

[2] K. Hock, E. Hamwi, F. Meot, H. Huang and V. Ptitsyn, *Simulations of polarized helions in the HSR*, in *Proc. IPAC'24*, no. 15 in International Particle Accelerator Conference, pp. 1634–1636, JACoW Publishing, Geneva, Switzerland, 7, 2024, DOI.

[3] H. Huang et al., *Strategy for proton polarization in the Electron Ion Collider*, in *Proc. IPAC'23*, no. 14 in International Particle Accelerator Conference, pp. 523–526, JACoW Publishing, Geneva, Switzerland, 9, 2023, DOI.

[4] V. Bargmann, L. Michel and V.L. Telegdi, *Precession of the polarization of particles moving in a homogeneous electromagnetic field*, *Phys. Rev. Lett.* **2** (1959) 435.

[5] Y.S. Derbenev and A.M. Kondratenko, *Acceleration of polarized particles to high energies in synchrotrons*, 10^{th} *International Conference on High Energy Accelerators* **10** (1977) 70.

[6] Y.S. Derbenev and A.M. Kondratenko, *On the Possibilities to Obtain High-Energy Polarized Particles in Accelerators and Storage Rings*, *AIP Conf. Proc.* **51** (1979) 292.

[7] G.H. Hoffstaetter, *Accelerator rings with polarized beams and spin manipulation*, in *1st Summer School and Workshop on COSY Physics (CSS 2002)*, pp. 85–126, 2002.

[8] D.P. Barber, J.A. Ellison and K. Heinemann, *Quasiperiodic spin-orbit motion and spin tunes in storage rings*, *Phys. Rev. ST Accel. Beams* **7** (2004) 124002.

[9] G. Hoffstaetter, M. Vogt and D. Barber, *Higher-order effects in polarized proton dynamics*, *Physical Review Special Topics-Accelerators and Beams* **2** (1999) 114001.

[10] K. Yokoya, *An Algorithm for calculating the spin tune in circular accelerators*, physics/9902068.

[11] G.H. Hoffstaetter, *Optimal axes of siberian snakes for polarized proton acceleration*, *Physical Review Special Topics—Accelerators and Beams* **7** (2004) 121001.

[12] G.H. Hoffstaetter, *High energy polarized proton beams: a modern view*, vol. 218, Springer Science & Business Media (2006).

[13] J. Berg et al., *Lattice design for the hadron storage ring of the Electron-Ion Collider*, in *Proc. IPAC'23*, no. 14 in International Particle Accelerator Conference, pp. 903–905, JACoW Publishing, Geneva, Switzerland, 9, 2023, DOI.

[14] E. Hamwi, G. Hoffstaetter, H. Huang, K. Hock and V. Ptitsyn, *Snake matching the EIC's hadron storage ring*, in *Proc. IPAC'24*, no. 15 in International Particle Accelerator Conference, pp. 1714–1717, JACoW Publishing, Geneva, Switzerland, 7, 2024, DOI.

[15] H.L. III et al., *Hadron Storage Ring 4 O'clock Injection Design and Optics for the Electron-Ion Collider*, in *Proc. IPAC'22*, no. 13 in International Particle Accelerator Conference, pp. 2068–2070, JACoW Publishing, Geneva, Switzerland, 7, 2022, DOI.

[16] H.L. III et al., *The Electron-Ion Collider Hadron Storage Ring 10 O'clock Switchyard Design*, in *Proc. IPAC'22*, no. 13 in International Particle Accelerator Conference, pp. 2071–2073, JACoW Publishing, Geneva, Switzerland, 7, 2022, DOI.

[17] D. Sagan, *Bmad: A relativistic charged particle simulation library*, *Nucl. Instrum. Meth.* **A558** (2006) 356.